Neuron
Article

The p150^{Glued} CAP-Gly Domain Regulates Initiation of Retrograde Transport at Synaptic Termini

Thomas E. Lloyd,[1,2,3,*] James Machamer,[2] Kathleen O'Hara,[1,3] Ji Han Kim,[2] Sarah E. Collins,[2] Man Y. Wong,[4] Brooke Sahin,[1,2] Wendy Imlach,[5] Yunpeng Yang,[2] Edwin S. Levitan,[4] Brian D. McCabe,[5] and Alex L. Kolodkin[1,3,*]
[1]The Solomon H. Snyder Department of Neuroscience
[2]Department of Neurology
[3]Howard Hughes Medical Institute
Johns Hopkins University School of Medicine, Baltimore, MD 21205, USA
[4]Department of Pharmacology and Chemical Biology, University of Pittsburgh, Pittsburgh, PA 15261, USA
[5]Departments of Pathology and Cell Biology and Neuroscience, Center for Motor Neuron Biology and Disease, Columbia University Medical Center, New York, NY 10032, USA
*Correspondence: tlloyd4@jhmi.edu (T.E.L.), kolodkin@jhmi.edu (A.L.K.)
DOI 10.1016/j.neuron.2012.02.026

SUMMARY

p150^{Glued} is the major subunit of dynactin, a complex that functions with dynein in minus-end-directed microtubule transport. Mutations within the p150^{Glued} CAP-Gly microtubule-binding domain cause neurodegenerative diseases through an unclear mechanism. A p150^{Glued} motor neuron degenerative disease-associated mutation introduced into the *Drosophila Glued* locus generates a partial loss-of-function allele (*Gl^{G38S}*) with impaired neurotransmitter release and adult-onset locomotor dysfunction. Disruption of the p150^{Glued} CAP-Gly domain in neurons causes a specific disruption of vesicle trafficking at terminal boutons (TBs), the distal-most ends of synapses. *Gl^{G38S}* larvae accumulate endosomes along with dynein and kinesin motor proteins within swollen TBs, and genetic analyses show that kinesin and p150^{Glued} function cooperatively at TBs to coordinate transport. Therefore, the p150^{Glued} CAP-Gly domain regulates dynein-mediated retrograde transport at synaptic termini, and this function of dynactin is disrupted by a mutation that causes motor neuron disease.

INTRODUCTION

Disruption of axonal transport is proposed to be a common mechanism in the pathogenesis of neurodegenerative diseases (De Vos et al., 2008; Perlson et al., 2010). Axonal microtubules (MTs) are polarized with their plus ends at synapses and their minus ends directed toward the soma. Anterograde cargo is transported to the synapse via microtubule plus-end-directed motors of the kinesin family, whereas retrograde transport is mediated via the minus-end-directed motor dynein (Kardon and Vale, 2009). However, it remains unclear how unidirectional transport is regulated at synapses and how the anterograde and retrograde transport machinery are coordinated.

Dynactin is a protein complex required for dynein-mediated microtubule-based transport. The p150^{Glued} dynactin subunit contains an aminoterminal *cytoskeleton-associated protein Gly-rich* (CAP-Gly) domain that is present in several microtubule plus-end tracking proteins (+TIPs). Interestingly, different missense mutations located within the p150 CAP-Gly domain cause two distinct adult-onset autosomal dominant neurodegenerative diseases: one resulting in motor neuron degeneration, termed hereditary motor neuropathy 7B (HMN7B) or distal spinal and bulbar muscular atrophy (Puls et al., 2003), and the other causing midbrain atrophy and loss of dopaminergic neurons without affecting motor neurons, termed Perry syndrome (Farrer et al., 2009). HMN7B is caused by a G59S missense mutation that inhibits the ability of dynactin to bind microtubules in vitro (Levy et al., 2006). *p150^{G59S}* transgenic mice develop progressive motor neuron degeneration with pathological similarities to Amyotrophic Lateral Sclerosis (ALS) (Chevalier-Larsen et al., 2008; Lai et al., 2007; Laird et al., 2008). It is intriguing that different mutations in the same domain of p150^{Glued} cause two dramatically distinct human neurodegeneration syndromes, and the mechanism by which these mutations disrupt p150^{Glued} function in neurons is unknown.

CAP-Gly domains interact with proteins that contain EEY/F motifs in their carboxyl (C) termini, including tyrosinated alpha-tubulin (Honnappa et al., 2006; Peris et al., 2006; Weisbrich et al., 2007). Although present diffusely along microtubules in most cell types, including neurons, a fraction of p150 protein localizes to microtubule plus ends in mammalian cells and in *Aspergillus* (Habermann et al., 2001; Vaughan et al., 1999, 2002; Zhang et al., 2003). However, deletion of the p150 microtubule-binding domain does not disrupt cargo transport in S2 cells, and *p150^{G59S}* transgenic mice do not have apparent defects in axonal transport (Chevalier-Larsen et al., 2008; Kim et al., 2007). Thus, although considerable evidence implicates dynactin in dynein-mediated microtubule-based transport, the function of dynactin and its microtubule-binding domain in regulating axonal transport is unclear.

The dynein/dynactin complex is highly conserved in *Drosophila*, and the p150 subunit, encoded by the *Glued* (*Gl*) gene, genetically interacts with dynein (McGrail et al., 1995; Waterman-Storer and Holzbaur, 1996). The p150 and arp1

dynactin subunits have been proposed to regulate both anterograde and retrograde transport of organelles in *Drosophila* axons (Haghnia et al., 2007; Pilling et al., 2006); however, the mechanism whereby dynactin coordinates bidirectional axonal transport is unknown. Gl^{1} is a spontaneously isolated *Glued* allele that causes truncation of the C-terminal third of the protein, and it functions genetically as a dominant-negative allele (referred to here as $p150^{\Delta C}$; see Figure S1A available online; Swaroop et al., 1985). In *Drosophila*, p150 is enriched at the larval neuromuscular junction (NMJ), and expression of $p150^{\Delta C}$ protein in motor neurons causes synapse instability and presynaptic retractions, leading to a reduction in bouton number and impaired neurotransmitter release at the NMJ (Allen et al., 1999; Eaton et al., 2002).

We characterize here disease-associated mutations in $p150^{Glued}$ that reveal a function for dynactin at the distal-most ends of synapses. Our data show that p150 and kinesin function synergistically at NMJ terminal boutons (TBs) to regulate dynein-mediated retrograde transport. We show that this function is specifically disrupted by a $p150^{Glued}$ mutation that causes motor neuron disease, but not by $p150^{Glued}$ mutations that cause Perry syndrome, suggesting that disruption of transport at synaptic termini contributes to the cell-type specificity of these diseases.

RESULTS

A Motor Neuron Disease-Causing Missense Mutation Produces a Partial Loss of *Glued* Function in *Drosophila*

The CAP-Gly microtubule-binding domain of $p150^{Glued}$ is phylogenetically conserved, including the residue mutated in HMN7B (Gly59 in human p150, corresponding to Gly38 in *Drosophila Glued*; Figure S1B). The *G59S* mutation in human p150 causes an ~50% reduction in binding of purified p150 microtubule-binding domain to microtubules in vitro (Levy et al., 2006). To determine how the corresponding *G38S* mutation in fly *Glued* affects microtubule binding in vivo, we purified microtubule-associated proteins from flies conditionally expressing hemagglutinin (HA)-tagged p150. Interestingly, whereas wild-type (WT) p150 cosediments with microtubules, as has been described for endogenous p150 (McGrail et al., 1995), the *G38S* mutant p150 protein exhibits a marked reduction in microtubule association (Figures 1A and S1C).

To investigate the consequences of the motor neuron disease-associated *G59S* mutation on *Glued* function in vivo, we first generated transgenic flies that express WT and mutant human and *Drosophila* p150 (Figure S1D). Surprisingly, overexpression of human or *Drosophila* $p150^{WT}$ in multiple independent transgenic lines is extremely toxic, leading to lethality or severe rough-eye phenotypes when overexpressed in neurons using the panneuronal driver $elav^{C155}$-*GAL4* (Figures 1B and 5C). In contrast, overexpression of human $p150^{G59S}$ or *Drosophila* $p150^{G38S}$ in neurons causes a mild rough-eye phenotype (Figure 1B), suggesting that the *G59S* mutation causes loss of function (LOF). Our biochemical data suggest that this LOF is due to a reduction in microtubule binding.

Whereas strong overexpression of $p150^{WT}$ is toxic, we found that low-level expression of *Drosophila* $p150^{WT}$ fully rescues the early larval lethality of *Glued* null animals ($Gl^{1-3}/Gl^{\Delta 22}$; Siller et al., 2005), demonstrating that these transgenes are fully functional (Figure 1E). Because the toxicity of high-level $p150^{WT}$ overexpression complicates the interpretation of $p150^{G38S}$ phenotypes, we introduced the *G38S* mutation directly into the endogenous *Glued* locus in the *Drosophila* genome by using homologous recombination (Figure 1C). This knockin approach generates an allelic replacement that changes only a single genomic DNA base pair without introducing exogenous DNA (hereafter referred to as Gl^{G38S}), thereby allowing the mutant gene to be expressed under the control of the normal *Glued* regulatory elements throughout all tissues and stages of development. Gl^{G38S} homozygous flies are viable but sterile, whereas $Gl^{G38S}/Gl^{null(1-3\ or\ \Delta 22)}$ flies are late pupal lethal, demonstrating that the Gl^{G38S} mutation is a hypomorphic allele of *Glued* (Figure 1E). The pupal lethality of Gl^{G38S}/Gl^{null} animals is fully rescued to adulthood with ubiquitous expression of $p150^{WT}$ or with a genomic fragment containing the *Glued* gene (BAC [Gl+]), demonstrating that this lethality is caused by loss of *Glued* function (Figure 1E). Western blot analysis shows that the mutant protein is expressed at reduced levels in Gl^{G38S} flies compared to controls, suggesting that the mutant protein is unstable (Figures 1D and S1E). A reduced level of mutant protein expression is also seen in mice in which the *G59S* mutation was introduced into the endogenous p150 locus (Lai et al., 2007).

Gl^{G38S} and $Gl^{G38S}/Gl^{\Delta 22}$ larvae exhibit normal locomotion (Figure 1F); however, Gl^{G38S} adult flies have dramatically impaired locomotor activity and are unable to fly (Figure 1G). Adult Gl^{G38S} animals develop progressive paralysis with age and have a markedly reduced lifespan (median survival 16 days versus 70 days in WT) (Figure 1H). The Gl^{G38S} early adult lethality and locomotor phenotypes are rescued with low-level expression of $p150^{WT}$ (Figures 1G and 1H), demonstrating that these phenotypes are due to a loss of *Glued* function. A similar, albiet less severe, locomotor phenotype is seen in the dominant-negative allele of *Glued* ($Gl^{1}/+$), confirming that disruption of *Glued* function in *Drosophila* causes age-dependent motor deficits and reduced survival (Figures S2A and S2B). Indeed, a reduction in lifespan is also observed after disruption of *Glued* function in all neurons, or specifically within motor neurons, by overexpressing either p150 protein lacking its C terminus ($p150^{\Delta C}$) or dynamitin (Dmn), the p50 subunit of the dynactin complex which disrupts the complex when overexpressed (Burkhardt et al., 1997) (Figure S2B). These data demonstrate that *Glued* function is required in motor neurons for normal locomotor function and life span.

Endosomes Accumulate at Terminal NMJ Boutons in Gl^{G38S} Animals despite Normal Axonal Transport

The dynactin complex regulates axonal transport in larval axons (Haghnia et al., 2007; Pilling et al., 2006), and disruption of axonal transport may underlie the pathogenesis of dynactin-mediated neurodegenerative diseases. Loss-of-function alleles in genes that encode dynein and dynactin subunits frequently display larval "tail-flip" phenotypes and "axonal jams" that can be labeled with synaptic vesicle markers, such as antibodies against synaptotagmin (Martin et al., 1999). Surprisingly, Gl^{G38S} animals do not display either of these phenotypes (Figure S3A

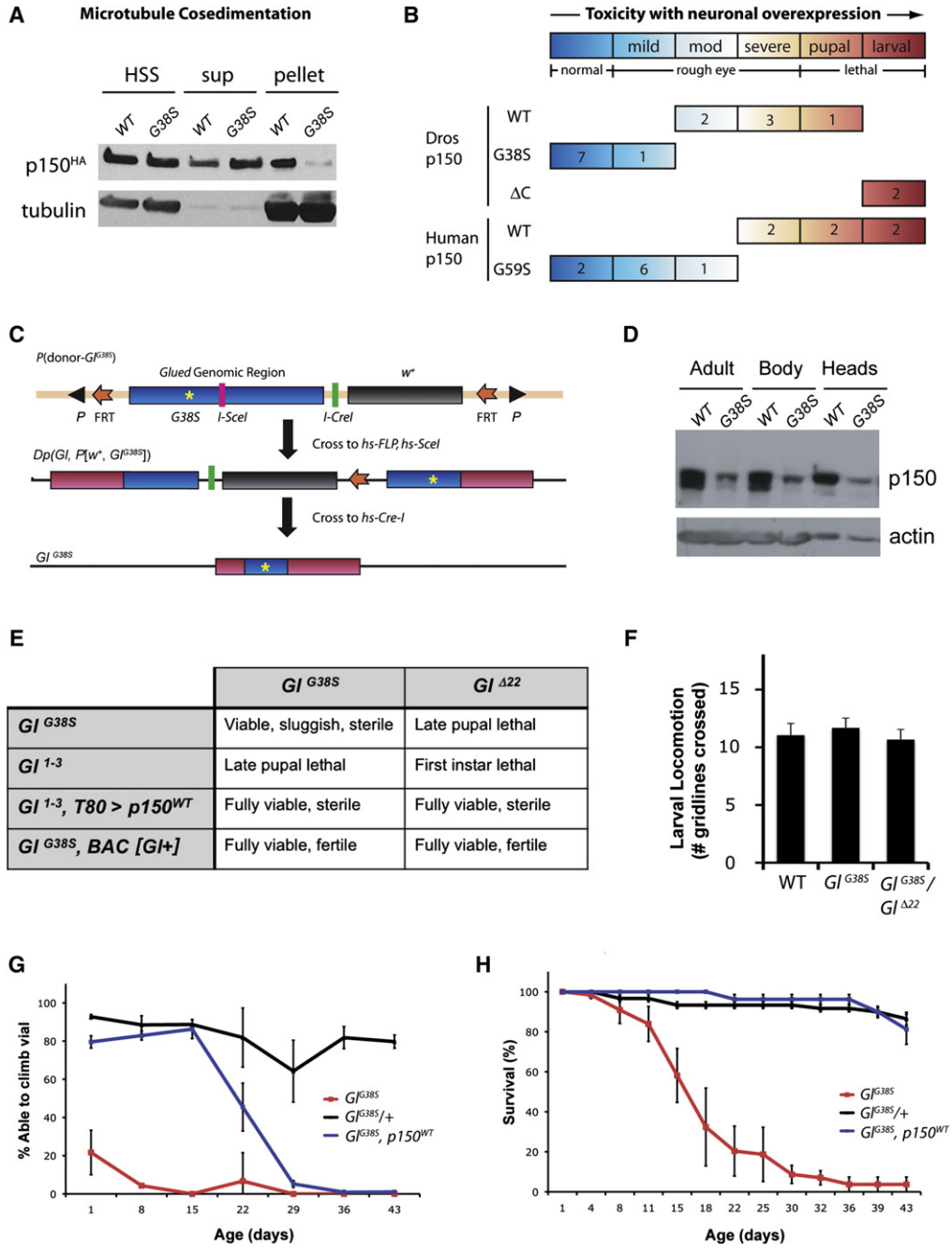

Figure 1. *Gl*^{G38S} Causes a Partial Loss of *Glued* Function

(A) p150^{G38S}-HA shows markedly reduced cosedimentation with microtubules in vivo. High-speed supernatants (HSS) from adult flies expressing WT or G38S HA-tagged p150 (p150^{HA}) under control of *hs-GAL4* were incubated with taxol and guanosine triphosphate to stabilize microtubules, and microtubules and associated proteins were purified by using ultracentriguation through a 15% sucrose cushion (see Figure S1C).

(B) Toxicity of p150 overexpression in fly neurons. Shown schematically are the gross phenotypes observed with *elav*^{C155}*-GAL4*-mediated overexpression of *UAS-p150* transgenic lines (number of lines with given phenotype in box; see also Figures S1A and S1B). The color scheme indicates severity of phenotype, with blue representing no observable phenotype and red signifying larval lethality.

(C) Targeting strategy for generating the *G38S* "knockin" allele of *Glued*. *P*(donor-*Gl*^{G38S}) denotes incorporation of the targeting construct within a P element onto the second chromosome. *Dp*(*Gl*, *P*[*w*$^{+}$, *Gl*^{G38S}]) indicates a line in which the endogenous *Glued* locus (red) has incorporated the mutated *Glued*-targeting construct (blue) to form a tandem duplication flanked by the *w*$^{+}$ gene. The bottom line indicates the resolution of the duplication after induction of Cre-I, leading to generation of the *Gl*^{G38S} allele (see Supplemental Experimental Procedures).

(D) Western blot analysis using an antibody directed against the p150 C terminus shows that protein levels are reduced in *Gl*^{G38S} animals. The antibody recognizes a doublet in whole adult flies and bodies but primarily recognizes a single band of 150 kDa in adult heads.

and data not shown), suggesting that axonal transport may not be severely disrupted. Because retrograde transport of Rab7(+)-signaling endosomes has been proposed to be disrupted in neurodegenerative diseases (Deinhardt et al., 2006; Perlson et al., 2010), we investigated the dynamics of endosomal axonal transport in Gl^{G38S} animals by imaging Rab7:green fluorescent protein (GFP) in larval segmental nerves (Figure 2A and Movies S1 and S2). Interestingly, though we see a decrease in the proportion of stationary Rab7:GFP particles in Gl^{G38S} animals (Figure 2B), all other axonal transport measures, including flux, velocity, and processivity, are unaffected (Figures 2C and 2D). We assayed retrograde signaling by the transforming growth factor (TGF)-beta receptor family member Wit, which is blocked in *Drosophila* overexpressing $p150^{\Delta C}$ (McCabe et al., 2003) and observed no reduction in pMad signaling in Gl^{G38S} larval motor neuron nuclei (Figure S3B). Taken together, these data suggest that retrograde axonal transport of endosomes occurs normally in Gl^{G38S} animals.

Overexpression of $p150^{\Delta C}$ causes a reduction in synaptic bouton number at the NMJ due to presynaptic retractions (Eaton et al., 2002). In contrast, Gl^{G38S} animals have a normal number of synaptic boutons in proximal abdominal segments (segments A2 and A3) and a small but significant increase in the number of synaptic boutons in distal segments (segments A5 and A6; Figures 2E and 2F). Surprisingly, when we look specifically at the distal-most synaptic boutons, TBs, we see an ~2-fold increase in bouton volume in distal segments. Interestingly, $p150^{WT\text{-}HA}$ expressed in motor neurons is dramatically enriched within NMJ TBs (Figure 2G, arrows), in addition to its expected localization along axons (Figure 2G, asterisks) and in the cytoplasm. We observe that the TB localization of $p150^{WT\text{-}HA}$ is apparently greatest within the center of the TB, just distal to where expression of the microtubule-associated protein Futsch becomes undetectable (Figure 2G). $p150^{WT\text{-}HA}$ is also enriched at sites of microtubule loops, which are thought to be enriched in microtubule plus ends (Figure 2G, arrowheads; enlarged in Figure S3C) (Roos et al., 2000). To determine whether microtubule plus ends are also enriched at TBs, we expressed a microtubule plus-end marker, the kinesin motor domain fused to GFP (Khc^{Head}:GFP) (Clark et al., 1994), in motor neurons. Interestingly, we see at the NMJ that Khc^{Head}:GFP is predominantly localized to the TB (Figures 2H and S3D) and, similar to $p150^{WT\text{-}HA}$ localization, is enriched within the middle of the TB (Figure 2H, inset). We also observe a similar enrichment of the microtubule plus-end marker EB1:GFP at this location (Movie S3). These data suggest that wild-type $p150^{Glued}$ is enriched at microtubule plus ends of terminal boutons.

Because $p150^{WT\text{-}HA}$ is localized within NMJ TBs, we next investigated the morphology of the presynaptic nerve terminal in *Glued* mutants. Anti-HRP labels the presynaptic membrane at the *Drosophila* NMJ and binds to neuron-specific transmembrane glycoproteins such as FasII (Desai et al., 1994). Interestingly, we observe intense anti-HRP staining within TBs of Gl^{G38S} and $Gl^{G38S}/Gl^{\Delta 22}$ NMJs (Figure 3A), suggesting that neuronal membranes accumulate at these presynaptic termini. Similar to the TB swelling we observed in $Gl^{G38S}/Gl^{\Delta 22}$ mutants, the anti-HRP phenotype is more severe in distal abdominal segments than in proximal segments (Figures 3A and 3D). Approximately 75% of NMJs from distal segments of Gl^{G38S} and $Gl^{G38S}/Gl^{\Delta 22}$ larvae display accumulation of anti-HRP staining within TBs, whereas only ~15% of control NMJs have any accumulation of anti-HRP staining within TBs (Figure 3D). Similarly, overexpression of $p150^{G38S}$ in motor neurons (using *D42-GAL4*) causes a dramatic accumulation of anti-HRP immunoreactivity in large puncta specifically located within the TB, demonstrating that $p150^{G38S}$ can act in a dominant-negative fashion when overexpressed in neurons (Figures 3B–3D). Because anti-HRP labels presynaptic transmembrane proteins, these data suggest that membrane-bound vesicles accumulate within TBs of Gl^{G38S} NMJs.

We next crossed *D42-GAL4, UAS-*$p150^{G38S}$ (*D42 >* $p150^{G38S}$) flies to flies that express fluorescently tagged markers that label distinct membrane-bound compartments under control of the *UAS* promoter. Colocalization of the membrane marker mCD8:GFP with anti-HRP in terminal boutons of larvae expressing $p150^{G38S}$ suggests that these anti-HRP positive structures are membrane bound (Figure 3C). Interestingly, the late endosome marker Rab7:GFP colocalizes with anti-HRP in TBs coexpressing both $p150^{G38S}$ and Rab7:GFP, suggesting that these membranous structures include endosomes (Figure 3B). Furthermore, transmembrane proteins known to cycle through endosomes, including synaptotagmin (Takei et al., 1996) and APP (Haass et al., 1992), also accumulate at these TBs and partially colocalize with anti-HRP (Figure 3C). Together, these data show that overexpression of $p150^{G38S}$ causes a marked accumulation of endosomal membranes and proteins at NMJ TBs.

To determine whether the accumulation of endosomes at *Glued* mutant TBs is due to disruption of dynein/dynactin function, we asked whether similar phenotypes are present in mutant alleles of genes encoding components of the dynein/dynactin complex. Because most available alleles are early larval or embryonic lethal, we knocked down dynein/dynactin subunits in motor neurons by using RNAi (Figure S4A). As expected, knockdown of three dynactin subunits (*Gl*, *cpa*, and *p62*) and three dynein subunits (*dhc*, *dic*, and *dlic*) phenocopies the TB accumulation of anti-HRP immunoreactivity and Syt:GFP that we observed in *D42 >* $p150^{G38S}$ animals (Figures 3C, 3E, and S4B). These data demonstrate that disruption of the dynein/dynactin complex causes an accumulation of endosomes within TBs of the NMJ.

(E) Complementation analyses demonstrate that the Gl^{G38S} allele is a partial loss-of-function (LOF) *Glued* allele. Gl^{1-3} and $Gl^{\Delta 22}$ are null alleles. *T80-GAL4* (a ubiquitous driver) in *trans* with *UAS-*$p150^{WT}$ rescues the first-instar larval lethality of Gl^{G38S}/Gl^{1-3} and $Gl^{\Delta 22}/Gl^{1-3}$ flies, though rescued adults are male and female sterile. An ~23 kb BAC (*CH322-82J07*) containing the entire *Glued* locus (*BAC [Gl+]*) fully rescues lethality and sterility of *Glued* animals.
(F) Gl^{G38S} larvae have normal locomotor activity, as indicated by the number of gridlines crossed per minute. n = 18 animals for each genotype.
(G and H) Gl^{G38S} adults exhibit progressive climbing deficits (G) and early lethality (H); this phenotype is rescued by ubiquitous expression of $p150^{WT}$ (*p150*^{WT} represents a transgenic *UAS-*$p150^{WT}$ line [#3] that drives constitutive expression). n > 50 flies per genotype. Error bars represent SEM.

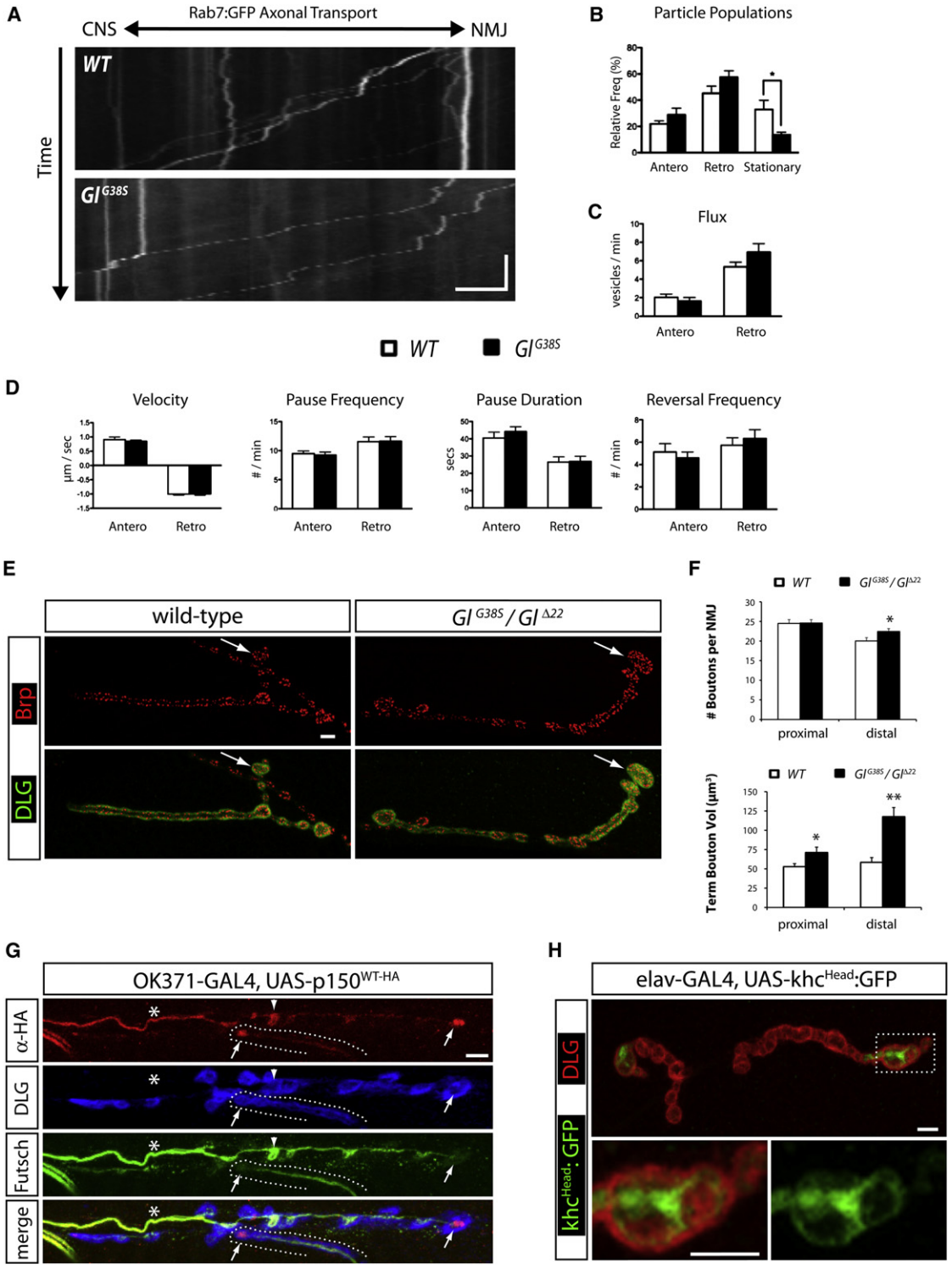

Figure 2. Terminal NMJ Bouton Phenotypes but Normal Axonal Transport in *Gl*^{G38S} Animals

(A) Representative kymographs of axonal transport of late endosomes in larval segmental nerves revealed by Rab7:GFP expressed in motoneurons. Central nervous system (CNS) is to the left and the NMJ is to the right. Time is on the y axis (scale bar represents 10 s) and proceeds from top to bottom.

(B) Population analysis of Rab7:GFP particles in *Gl*^{G38S} animals demonstrates a reduced frequency of stationary endosomes along axons.

(C) The number of endosomes that move along axons per minute (flux) is not altered in *Gl*^{G38S} animals.

(D) Analysis of Rab7:GFP kinetics demonstrates no difference in the velocity or processivity (pause frequency, duration, or reversal frequency) in *Gl*^{G38S} animals. n = 7 animals; 24–48 vesicles per animal.

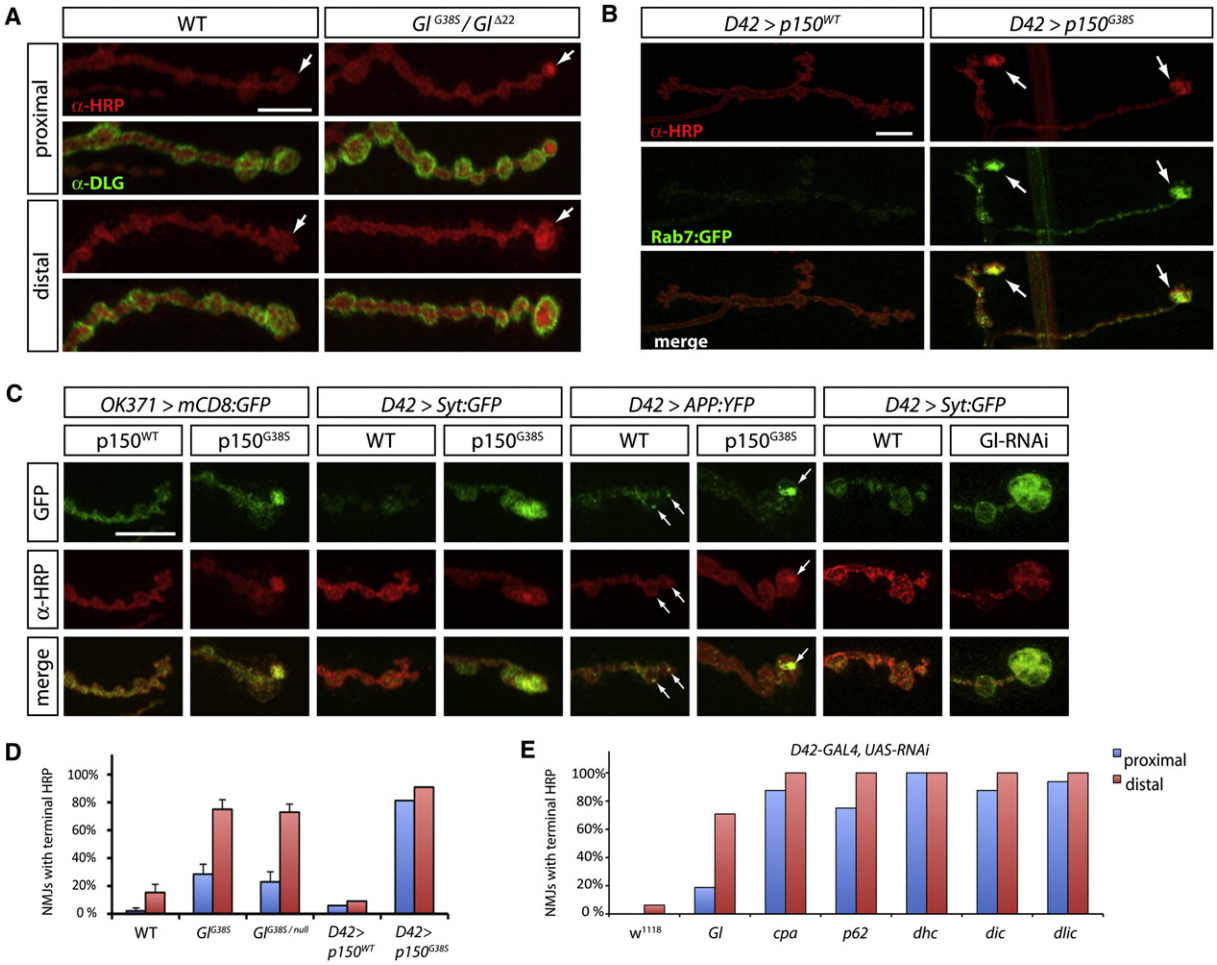

Figure 3. Endosomes Accumulate at Terminal NMJ Boutons in Gl^{G38S} Mutant Larvae

(A) Neuronal membranes (labeled with anti-HRP) accumulate within TBs (arrows) of proximal (A2) and distal (A6) segments in $Gl^{G38S}/Gl^{\Delta 22}$ larvae.

(B) Co-overexpression of Rab7:GFP with $p150^{G38S}$ in motor neurons using *D42-GAL4* demonstrates colocalization of anti-HRP staining with Rab7:GFP.

(C) TB accumulation of anti-HRP partially colocalizes with mCD8:GFP (labeling membranes), synaptotagmin:GFP (Syt:GFP), and APP:YFP and is also seen with RNAi-mediated knockdown of *Glued* (enhanced with coexpression of UAS-Dcr2). APP-YFP is often present in small anti-HRP+ puncta at TBs of wild-type animals (arrows).

(D and E) Quantitation of the TB anti-HRP accumulation phenotype in different genotypes (D) and with RNAi-mediated knockdown (E) of dynactin subunits; *Glued*, *Gl*; *capping protein alpha*, *cpa*; *p62* (*CG12042*); *Dynein heavy chain 64C*, *dhc*; *Dynein intermediate chain*, *dic*; and *Dynein light intermediate chain*, *dlic*. n > 6 animals (24 synapses) for each genotype. In Gl^{G38S} animals and animals with *Gl*-RNAi, the TB anti-HRP accumulation is more severe in distal segments. Scale bar represents 10 μm. Error bars represent SEM.

Dynein Heavy Chain Accumulates at Gl^{G38S} Terminal Boutons

In filamentus fungi, the dynactin complex is required for MT plus-end localization of dynein and for the interaction between dynein and endosomes (Xiang et al., 2000; Zhang et al., 2010). To determine whether dynein is mislocalized in *Glued* animals, we analyzed the expression of the cytoplasmic dynein heavy chain (cDhc64C, referred to here as Dhc). Surprisingly, Gl^{G38S} larvae

(E) NMJs develop normally in $Gl^{G38S}/Gl^{\Delta 22}$ third-instar larvae, with normal appearance of active zones (labeled with Brp); however, TBs are swollen (arrows). Segment A6 is shown.

(F) Top: quantification of type Ib bouton number per hemisegment in proximal (A2 and A3) and distal (A5 and A6) segments in wild-type and $Gl^{G38S}/Gl^{\Delta 22}$ animals. n = 10 animals each. Bottom: TB volume is increased in $Gl^{G38S}/Gl^{\Delta 22}$ animals compared with wild-type, and the TB volume of distal segments is increased relative to proximal segments (p = 0.004). n = 17 synapses from 5 animals of each genotype.

(G) $p150^{HA}$, when expressed in motor neurons under control of *OK371-GAL4*, is enriched at microtubule plus ends at NMJ TBs (arrows) and throughout axons (asterisks). A muscle 6-7, segment A3, NMJ is shown; dotted lines outline a type Is NMJ, and arrowheads label a type Ib NMJ. p150 is also enriched in microtubule loops (arrowhead, Figure S3D).

(H) TBs are enriched in microtubule plus ends. Expression of the motor domain of Khc fused to GFP (Khc^{Head}:GFP) leads to expression of GFP specifically within the NMJ TB (see inset and also Figure S3B). Scale bar represents 5 μm. *p < 0.05; **p = 0.0003. Error bars represent SEM.

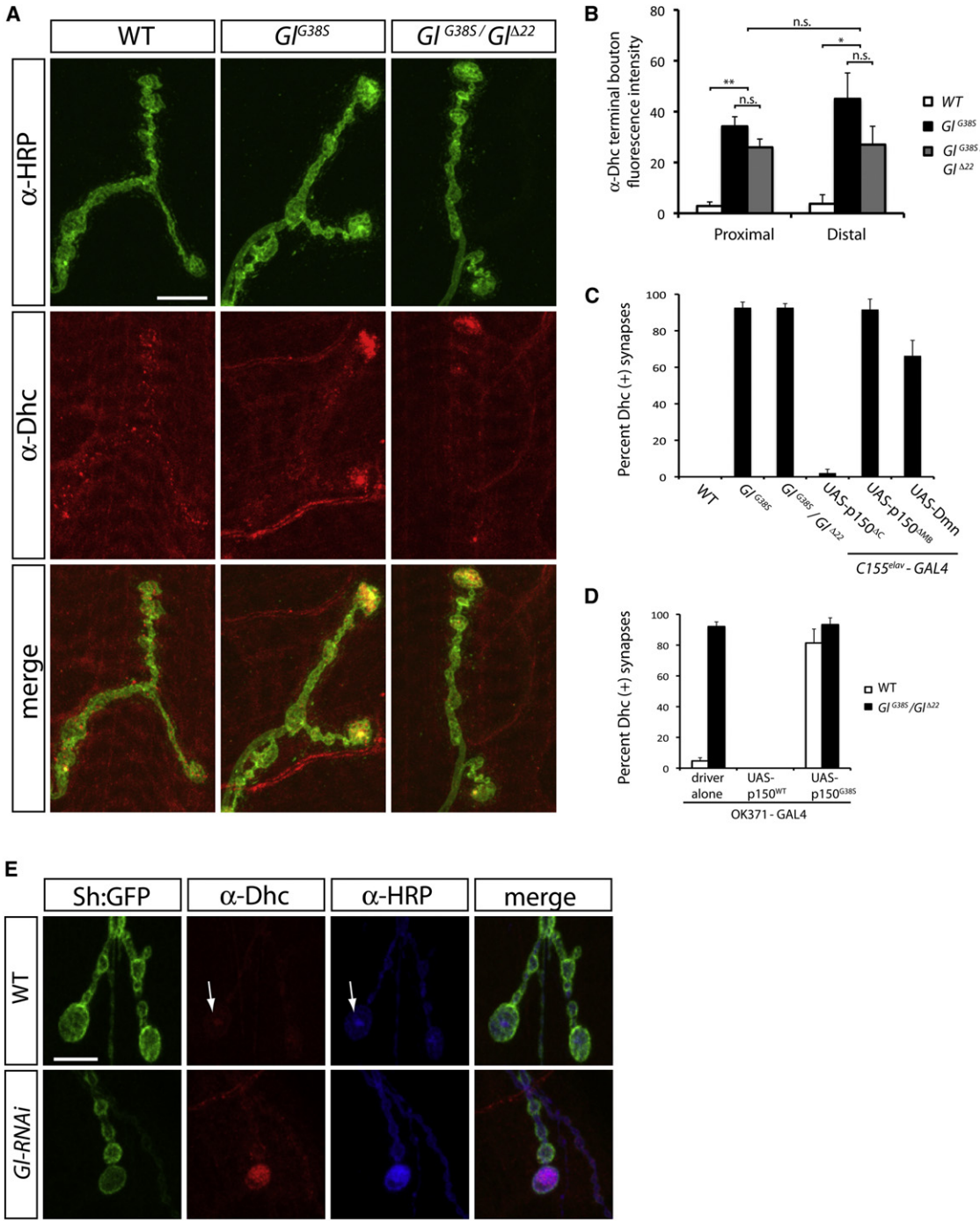

Figure 4. Dynein Is Mislocalized to the Terminal NMJ Bouton in *Gl*^{G38S} Mutants

(A) Dynein heavy chain (Dhc) is mislocalized to NMJ TBs (labeled with anti-HRP) in *Gl*^{G38S} mutant animals.

(B) Quantification of Dhc fluorescence intensity in the TB of proximal (A2 and A3) and distal (A6) segments.

(C and D) Quantification of Dhc TB accumulation indicated as mean percentage of Dhc (+) synapses. n > 40 synapses from 5 animals for each genotype.

(E) *Gl*-RNAi larvae are of the genotype *UAS-Dcr2/+; OK371-GAL4/UAS-Gl-RNAi; MHC:Sh-GFP*. Sh:GFP expressed in muscles labels the postsynaptic density. Scale bar represents 10 μm. *p < 0.01; **p < 0.0001; n.s., not significant. Error bars represent SEM.

reveal a striking accumulation of Dhc at NMJ TBs in all segments in 100% of *Gl*^{G38S} and *Gl*^{G38S}/*Gl*$^{\Delta 22}$ animals; this phenotype is never observed in wild-type animals (Figures 4A–4C and Figures S5A and S5B). At wild-type synapses, Dhc is localized to small puncta at the periphery of all boutons (Figure 4A), and occasionally small Dhc(+) puncta are observed near the center of the TB

(Figure 4E, arrow). In Gl^{G38S} animals, however, the mean Dhc signal intensity is increased ~10-fold within TBs, with no significant differences between proximal and distal segments (Figure 4B). Interestingly, in Gl^{G38S} larvae, Dhc predominantly accumulates at TBs of the longest branch in synapses with multiple branches (Figures S5A and S5B). These accumulations are not seen in axons or motor neuron cell bodies (Figure S5B and data not shown). Microtubules do not appear to be altered at Gl^{G38S} NMJs; however, we did note that mutant TBs with observable microtubule bundles did not accumulate dynein (Figure S5C, arrow), in contrast to those TBs with no significant tubulin staining. These data suggest that dynein accumulates in Gl^{G38S} TBs lacking stable microtubules.

The accumulation of Dhc specifically within the TB of Gl^{G38S} NMJs is consistent with an inability of the Dhc motor to move retrogradely at TBs. To further investigate dynein function at TBs, we quantified this phenotype in different mutant backgrounds. In Gl^{G38S} or $Gl^{G38S}/Gl^{\Delta 22}$ animals, ~90% of NMJs have marked TB accumulation of Dhc, whereas 0% of synapses from WT animals exhibit this phenotype (Figure 4C). This phenotype is fully rescued by motor neuron-specific expression of $p150^{WT}$, but not $p150^{G38S}$ (Figure 4D), showing that it is neuron autonomous and due to a loss of *Glued* function. A similar phenotype is observed after disruption of the dynactin complex with *Glued* RNAi or dynamitin overexpression (Figures 4C and 4E), further demonstrating that dynein accumulation is due to loss of dynactin function. Furthermore, overexpression of $p150^{G38S}$, or an amino-terminal deletion mutant protein lacking the CAP-Gly domain ($p150^{\Delta MB}$), causes a similar dynein mislocalization phenotype; however, this is not observed after overexpression of $p150^{\Delta C}$. These findings demonstrate that disruption of the $p150^{Glued}$ CAP-Gly domain, but not overexpression of $p150^{\Delta C}$ (commonly used in *Drosophila* to disrupt *Glued* function), causes Dhc accumulation at TBs. Because overexpression of $p150^{G38S}$ phenocopies *Glued* RNAi, the *G38S* mutation likely functions in a dominant-negative fashion when overexpressed in motor neurons.

To determine whether dynein mislocalization at synaptic termini is specific to motor neurons in *Glued* animals, we overexpressed $p150^{G38S}$ in sensory neurons and analyzed its effect on dynein localization. Ppk^{+} multidendritic sensory neuron presynaptic termini (labeled with synaptotagmin:GFP) are distributed in a stereotypical arrangement within the neuropil of the ventral nerve cord (Figure S6A). Interestingly, overexpression of *Drosophila* $p150^{G38S}$, or human $p150^{G59S}$, causes a dramatic accumulation of Dhc within all sensory presynaptic termini (Figure S6B), and a similar phenotype is seen in Gl^{G38S} animals (data not shown). Whereas axons in *Drosophila* and vertebrates are oriented with their microtubule plus ends distally, in *Drosophila*, dendritic MTs are oriented with their minus ends distal (Rolls et al., 2007). Consistent with our data suggesting that $p150^{Glued}$ plays a role in dynein-mediated retrograde transport at microtubule plus ends, Dhc is not mislocalized to ends of sensory dendrites (Figure S5B, arrows). Furthermore, we do not observe Dhc accumulation at the base of dendrites containing microtubule plus ends (Figure S5B, box). These data demonstrate that loss-of-function mutations in $p150^{Glued}$ that disrupt microtubule-binding lead to an accumulation of dynein at presynaptic termini.

kinesin heavy chain Functions Synergistically with *Glued* at Terminal Boutons

To further understand the molecular basis of *Glued* dysfunction in mutant neurons, we performed a candidate-based screen for modifiers of Gl^{G38S} lethality. We identified a null allele of the Kinesin-1 family member *kinesin heavy chain* (khc^{8}) as a potent enhancer of Gl^{G38S} lethality (Figures 5A and 5B). Conversely, the khc^{8} allele markedly suppresses the rough-eye phenotype we observe after overexpression of wild-type p150 in the *Drosophila* eye driven by *GMR-Gal4* (Figure 5C). These data suggest that *Glued* and *khc* function cooperatively, not antagonistically, as would be predicted if they simply regulated microtubule-based transport in opposite directions. A cooperative role for kinesin and dynactin has been proposed (Deacon et al., 2003; Gross et al., 2002; Haghnia et al., 2007; Martin et al., 1999); however, the molecular mechanism of this synergistic interaction is unclear.

One potential mechanism underlying cooperativity between *khc* and *Glued* is that kinesin-mediated delivery of p150 to microtubule plus ends at synaptic termini may be rate limiting for the initiation of retrograde transport. In *Aspergillus*, kinesin is required for plus-end localization of dynein and dynactin (Zhang et al., 2003), and the dynein/dynactin complex is anterogradely transported along axons in vertebrates via KIF5, the ortholog of Khc (Hirokawa et al., 2010). Strikingly, whereas Khc is present at very low levels at wild-type NMJs, it accumulates both at TBs in Gl^{G38S} animals and also after presynaptic knockdown of dynactin subunits (Figures 5D and S7). This pattern of Khc mislocalization is similar to the Dhc mislocalization we observe in these mutants and, indeed, Khc colocalizes with Dhc at Gl^{G38S} TBs (Figure 5E); all TBs with significant Dhc accumulation also show Khc accumulation. We do not see accumulation of Khc or Dhc along motor and sensory axons in larval segmental nerves (Figure S5A and data not shown), showing that this phenotype specifically occurs at synapses. These data suggest that $p150^{Glued}$ coordinates Khc-mediated anterograde transport with Dhc-mediated retrograde transport at TBs.

To test whether $p150^{Glued}$ and kinesin function cooperatively at synapses, we investigated genetic interactions between khc^{8} and Gl^{G38S}. There is a dramatic enhancement of the Gl^{G38S} TB swelling and anti-HRP accumulation phenotypes at all NMJs in all segments when *khc* gene dosage is reduced by 50% (Figures 5F and 5G), and the severity of the $khc^{8}/+$; $Gl^{G38S}/+$ phenotype is similar to the Gl^{G38S} homozygous phenotype. Furthermore, the distribution of anti-HRP localization within TBs of $khc^{8}/+$; Gl^{G38S} NMJs is similar to the localization of Khc^{Head}:GFP when it is expressed in wild-type motor neurons (Figure 2B). These data suggest that kinesin functions with p150 in TBs to coordinate bidirectional vesicle transport.

$p150^{G38S}$ Disrupts Retrograde Transport from Terminal Boutons and Synaptic Transmission

To directly investigate $p150^{Glued}$-mediated regulation of retrograde transport at synaptic termini, we monitored dense core vesicle (DCV) retrograde transport at TBs in larvae overexpressing $p150^{G38S}$. DCVs are more uniform in size than endosomes, and single vesicles can be imaged at the NMJ in real time by

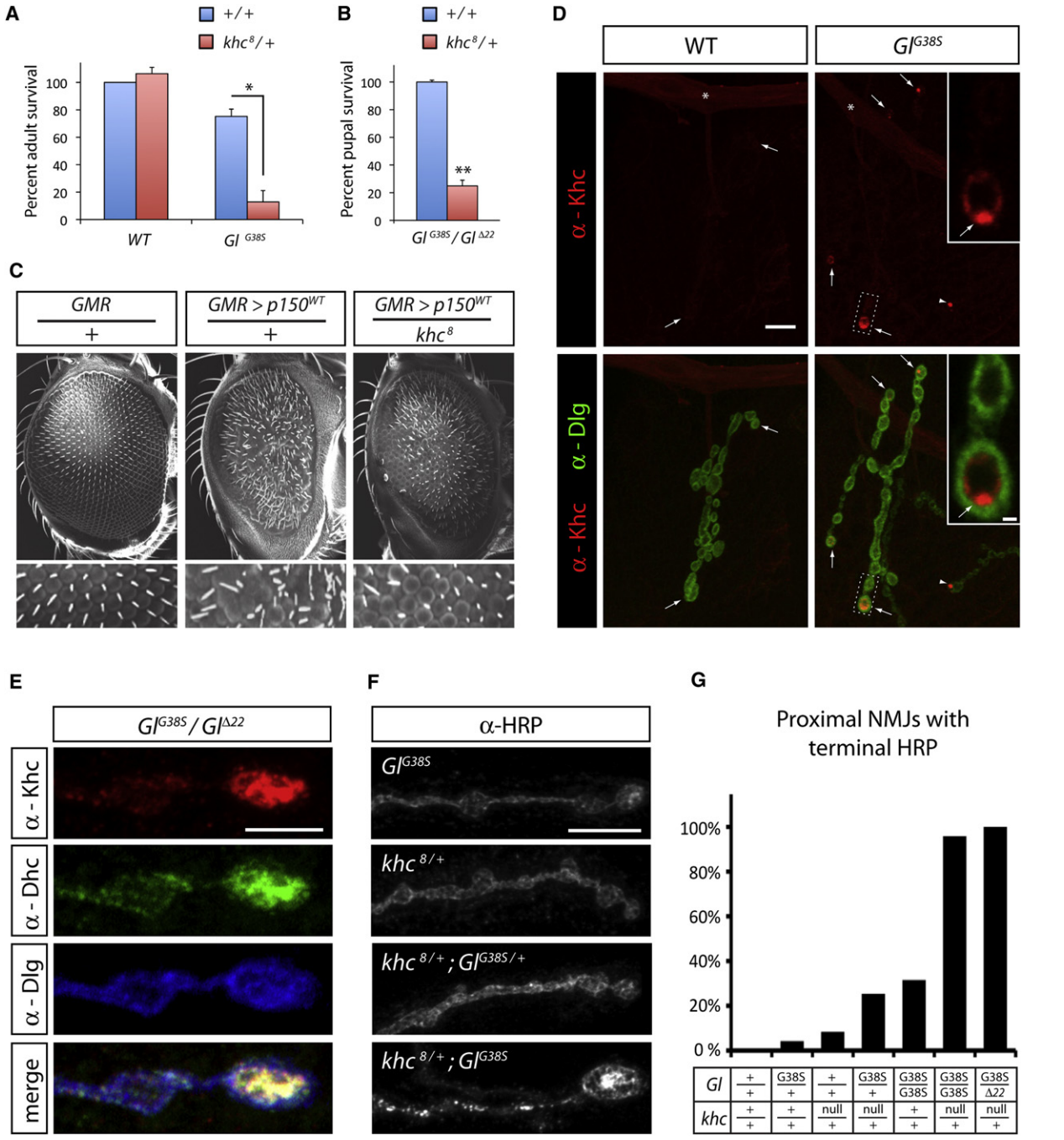

Figure 5. Kinesin Heavy Chain Functions Synergistically with *Glued* at NMJ Terminal Boutons

(A) A 50% reduction in gene dosage of the anterograde microtubule motor *kinesin heavy chain* (*khc*) markedly enhances lethality of Gl^{G38S} animals.

(B) $Gl^{G38S}/Gl^{\Delta 22}$ animals rarely survive to pupal stages when heterozygous for null *khc* ($khc^{8}/+$).

(C) Overexpression of $p150^{WT}$ in the eye with *GMR-Gal4* (*GMR* > $p150^{WT}$) causes a severe rough-eye phenotype that is suppressed with a reduction in *khc* dosage. SEM images of the eye are shown with enlargements below. Note the severe fusion of ommatidia and bristle disorganization in *GMR* > $p150^{WT}$ / + animals that is suppressed in *GMR* > $p150^{WT}$ / khc^{8}.

(D) Khc is expressed diffusely in axons (asterisks) and the NMJ in wild-type animals, whereas it accumulates at TBs (arrows) of Gl^{G38S} animals. Inset shows magnification of boxed area (scale bar represents 1 μm), with Khc accumulation at the periphery of the TB.

(E) Kinesin and Dynein colocalize at TBs of $Gl^{G38S}/Gl^{\Delta 22}$ animals.

(F and G) Genetic interaction between *khc* and *Glued* at TBs. Graph shows percentage of NMJs from segments A2 and A3 with TB accumulations of anti-HRP. n > 24 synapses from >6 animals of each genotype. Scale bar represents 10 μm in (D) and 5 μm in (E) and (F). *p = 0.003; **p < 0.0001. Error bars represent SEM.

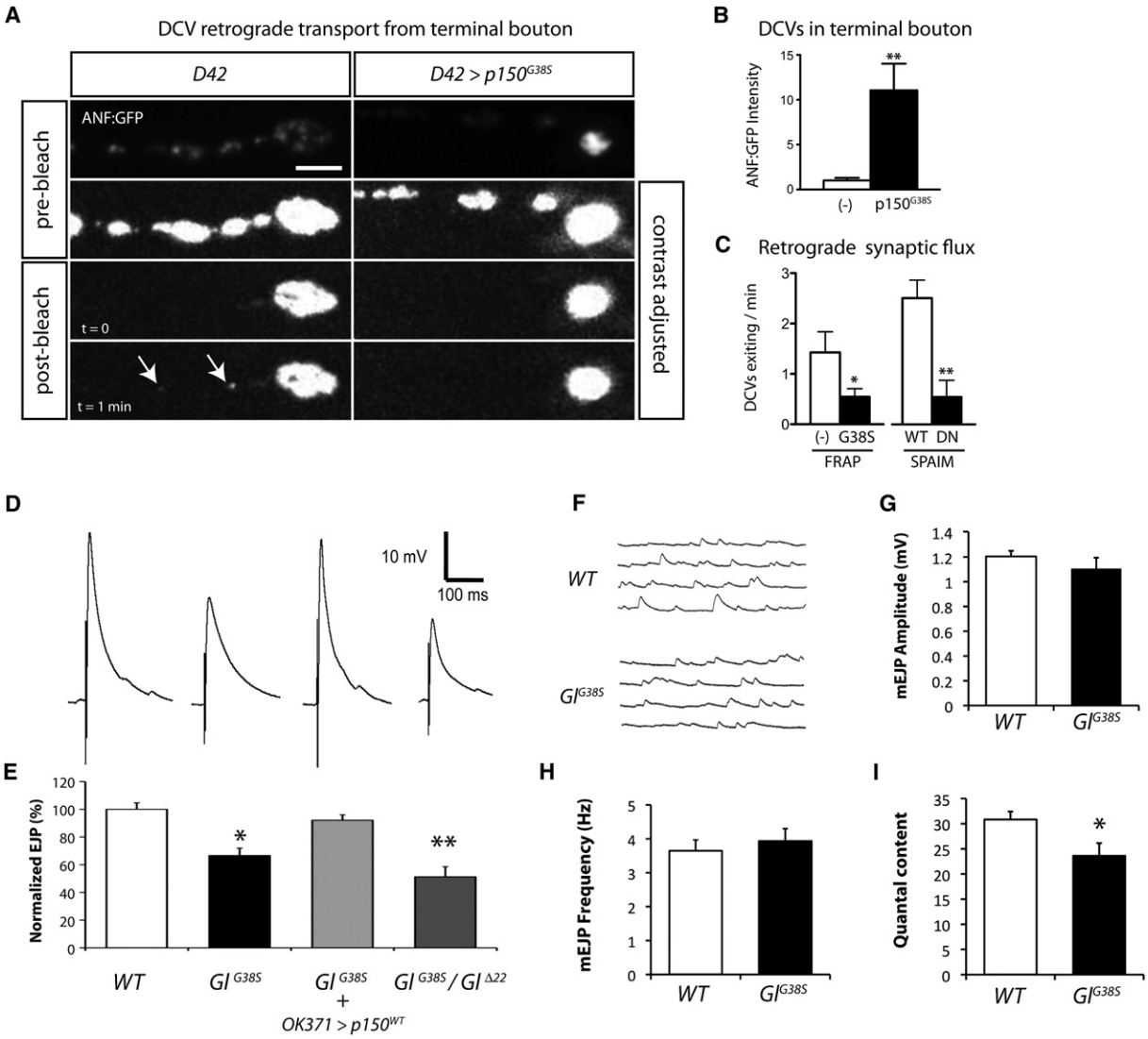

Figure 6. p150^{G38S} Disrupts Retrograde Transport at TBs and Neurotransmitter Release

(A and B) Retrograde synaptic dense core vesicle (DCV) transport from TBs is impaired by overexpression of p150^{G38S}.

(A) Top: *D42* control (left: *elav^{C155}-GAL4/Y*; *UAS-ANF:GFP / D42-GAL4*) larval NMJs distribute DCVs (marked by ANF:GFP) throughout synaptic boutons, whereas *D42 > p150^{G38S}* (right: *elav^{C155}-GAL4/Y; UAS-ANF:GFP / D42-GAL4, UAS-p150^{G38S}*) larval NMJs accumulate DCVs at TBs. After adjusting contrast to visualize individual DCVs (bottom three panels), all boutons except for the TB were bleached (t = 0), and single DCVs were imaged exiting the TB. Scale bar represents 10 μm.

(B) Quantitation of ANF:GFP intensity reveals an ~10× increase in DCVs in TBs of *D42 > p150^{G38S}* animals. n = 6 animals.

(C) Quantitation of DCV transport from TBs (retrograde synaptic flux) demonstrates a significant impairment in retrograde DCV flux from the TB with disruption of dynactin. Left: data from FRAP experiments; right: SPAIM results. n > 7 animals for (−) control (*D42* alone), G38S (*D42 > p150^{G38S}*), WT (*elav^{C155} > p150^{WT}*), and dominant negative (DN) (*elavGS > p150^{4C}*). *p < 0.05; **p < 0.01.

(D and E) Electrophysiology at the third-instar larval NMJ demonstrates that EJP amplitude is reduced in *Gl^{G38S}* mutant animals (n = 12 animals; *p = 1 × 10^{-4}; **p = 1 × 10^{-5}).

(F–I) Spontaneous neurotransmitter release (mEJP amplitude and frequency) is not affected in *Gl^{G38S}* larvae.

(I) The reduction in *Gl^{G38S}* EJP amplitude is due to reduced quantal content (*p = 0.03). Error bars represent SEM.

using ANF:GFP as a marker (Levitan et al., 2007). Similar to what we observe for Rab7:GFP, overexpression of p150^{G38S} causes a dramatic accumulation of DCVs at TBs (Figures 6A, top, and 6B). After photobleaching of wild-type (*D42* driver alone) proximal NMJ boutons, individual DCVs rapidly exit the TB (Movie S4 and Figure 6A, bottom). Despite an ~10-fold increase in ANF:GFP fluorescence intensity at the terminal bouton in mutant animals (Figure 6B), ~3-fold fewer vesicles undergo retrograde transport from the terminal bouton (Movie S5 and Figure 6C). Similar effects are seen after overexpression of

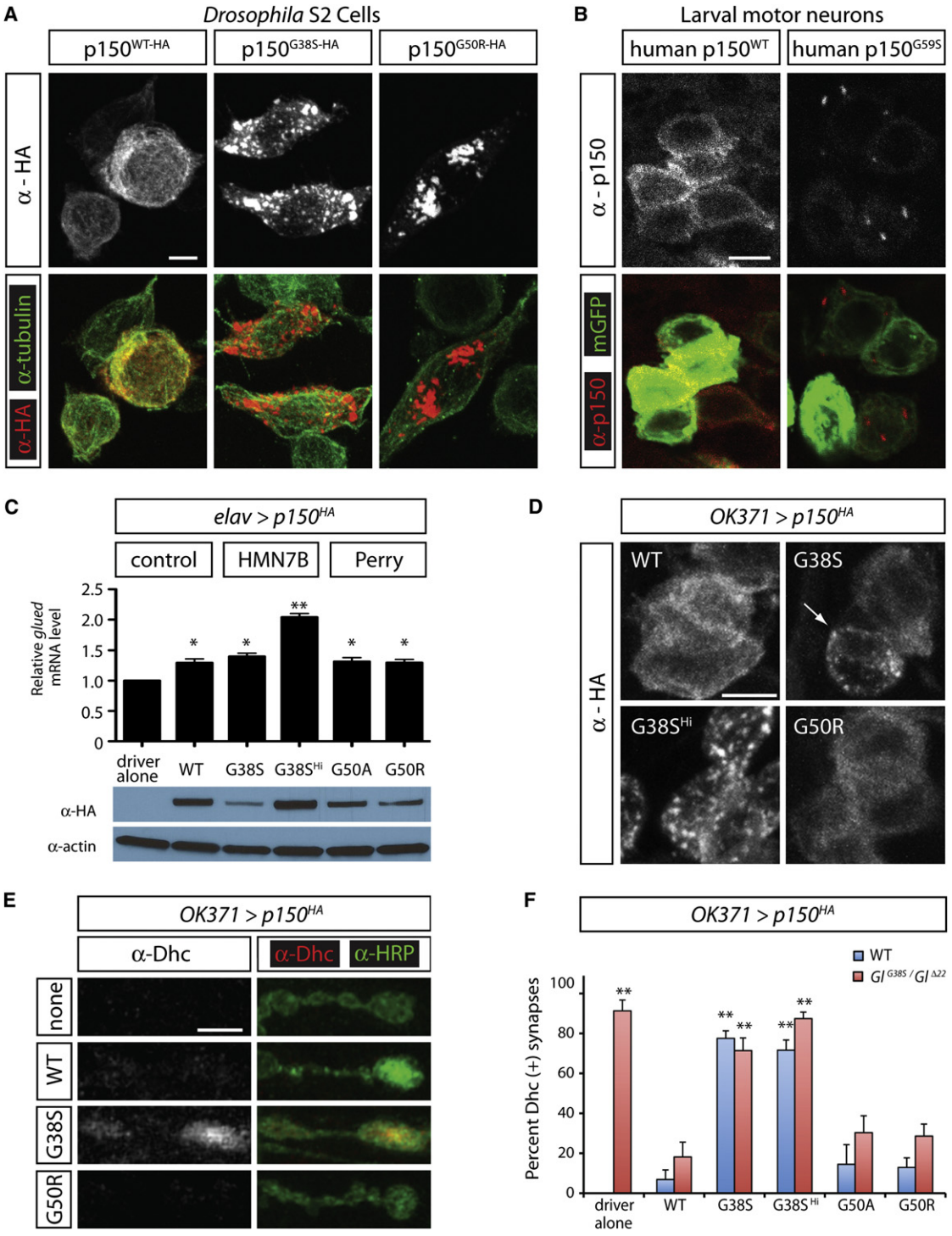

Figure 7. Aggregates within Motor Neurons and Dynein Mislocalization Is Specific to *p150* Mutations that Cause HMN7B, but Not Perry Syndrome

(A) In S2 cells, HA-tagged p150^{WT} is diffusely present in the cytoplasm and partially colocalizes with microtubules (labeled with antitubulin). Mutant p150 proteins (G38S and G50R) form large cytoplasmic aggregates in cells.

(B) Human p150^{WT} localizes diffusely throughout the cytoplasm in *Drosophila* motor neurons when expressed with *OK371-GAL4*, whereas human p150^{G59S} forms large cytoplasmic aggregates. *mCD8:GFP* (mGFP) labels motor neuron membranes.

(C) *mRNA* and protein expression of HA-tagged p150 in fly heads of transgenic lines using *elav-GAL4*. qRT-PCR shows that *WT*, *G38S*, *G50A*, and *G50R* transgenic lines all express similar increased levels of *glued* mRNA compared with drive alone, whereas the *G38S^{Hi}* line expresses much higher levels. Western

dominant-negative Glued ($p150^{\Delta C}$) by using a novel imaging approach termed SPAIM (*simultaneous photobleaching and imaging*) (Wong et al., 2012) to specifically visualize retrograde vesicle transport at TBs (Figure 6C). These data directly demonstrate that disruption of dynactin inhibits retrograde transport of DCVs from TBs.

Terminal NMJ boutons in *Drosophila*, as compared to proximal boutons, exhibit markedly enhanced synaptic transmission (Guerrero et al., 2005). To determine whether the disease-associated Gl^{G38S} mutation causes a defect in synaptic transmission, we performed electrophysiological analyses on Gl^{G38S} animals at the third-instar larval NMJ. Gl^{G38S} animals exhibit a significant reduction in the amplitude of evoked junctional potential (EJP) (Figures 6D and 6E), and this impairment in evoked synaptic transmission is fully rescued by presynaptic expression of wild-type p150. Therefore, this defect is due to loss of *Glued* function in motor neurons. We observe no change in the frequency or amplitude of miniature EJPs (mEJPs), showing that spontaneous neurotransmitter release is unaffected in Gl^{G38S} animals (Figures 6F–6H). These results show that Gl^{G38S} animals have a reduction in the quantal content of evoked neurotransmitter release at the NMJ (Figure 6I), despite the presence of a normal number of synaptic boutons at these terminals.

Perry and HMN7B Mutant p150 Proteins Affect Distinct p150 Functions within Motor Neurons

Perry syndrome is characterized by degeneration of neurons within the substantia nigra and brainstem; however, it does not noticeably affect motor neurons (Farrer et al., 2009). Remarkably, Perry syndrome, like HMN7B, is also caused by mutations in the CAP-Gly domain of p150 (Figure S1B). Therefore, to gain insight into the cell-type specificity of neurodegeneration caused by different mutations in the p150 CAP-Gly domain, we assessed whether functional differences exist in *Drosophila* between the HMN7B mutation (G38S) and Perry syndrome mutations (G50A and G50R). When expressed in *Drosophila* S2 cells (Figure S8A), both $p150^{G38S}$ and $p150^{G50R}$ form large cytoplasmic puncta (Figure 7A), similar to the protein aggregates seen in patients with these diseases. In contrast, the wild-type protein does not form large puncta in S2 cells and is present diffusely in the cytoplasm. Interestingly, we observe a similar appearance of puncta in *Drosophila* motor neurons after overexpression of human $p150^{G59S}$, whereas human $p150^{WT}$ is diffusely expressed in the motor neuron cell body cytoplasm (Figure 7B). To directly compare the effects these different disease mutations have on p150 function in vivo, we utilized transgenic animals that express different HA-tagged p150 proteins at equivalent levels, employing site-specific chromosomal integration (Bischof et al., 2007). When these transgenes are expressed under the control of *elav-GAL4*, Perry (*G50A* and *G50R*) and HMN7B (*G38S*) mutations cause a reduction in p150 protein expression in vivo compared with wild-type p150 expression, despite equivalent mRNA levels (Figure 7C). These data suggest that both HMN7B and Perry mutations cause the protein to be unstable, as is suggested by the reduced p150 protein levels we observe in Gl^{G38S} flies (Figure 1D). We generated a high-level-expressing transgenic line ($G38S^{Hi}$) that expresses $p150^{G38S}$ mutant protein at levels at least as high, if not higher, than wild-type p150 (Figure 7C), and this line was used to control for protein expression.

Similar to what we observed in S2 cells and motor neurons after expression of human $p150^{G59S}$, when $p150^{G38S\text{-}HA}$ is expressed in motor neurons using the *OK371-GAL4* driver, we find large puncta within motor neuron cell bodies, whereas $p150^{WT\text{-}HA}$ is diffusely present in the motor neuron cytoplasm (Figures 7D and S8B). In the $G38S^{Hi}$ line, all motor neurons show p150-HA(+) puncta, and many are very large (Figures 7D and S8B); in the low-expressing line, however, large puncta are rarely observed (seen in at least two motor neurons in five out of six animals). In contrast, large puncta are not detected in $p150^{G50A\text{-}HA}$ or $p150^{G50R\text{-}HA}$ animals (no puncta seen in six animals each, Figures 7D and S8B). Because large puncta were detected in $p150^{G38S\text{-}HA}$ animals that express lower levels of p150 protein (but equivalent mRNA levels) compared with $p150^{G50A\text{-}HA}$ or $p150^{G50R\text{-}HA}$ animals, we conclude that, within motor neurons, the HMN7B mutation makes p150 more aggregate prone than the Perry mutations.

To determine whether Perry syndrome mutations cause dynein-mislocalization phenotypes similar to those we observe in HMN7B (Gl^{G38S}) mutant animals, we overexpressed wild-type and mutant $p150^{HA}$ proteins in motor neurons. Overexpression of $p150^{HA}$ causes significant toxicity, similar to what we observed with high-level overexpression of untagged p150, as evidenced by a reduction in bouton number, abnormal synapse morphology, appearance of axonal swellings (data not shown), and accumulation of anti-HRP within the terminal bouton (Figure 7E). However, we only observed TB accumulation of Dhc after $p150^{G38S\text{-}HA}$ overexpression (Figures 6E and 6F); there was no difference in Dhc distribution among larvae overexpressing $p150^{WT\text{-}HA}$, $p150^{G50A\text{-}HA}$, or $p150^{G50R\text{-}HA}$. Furthermore, motor neuron-specific expression of $p150^{WT\text{-}HA}$, $p150^{G50A\text{-}HA}$, and $p150^{G50R\text{-}HA}$, but not $p150^{G38S\text{-}HA}$, rescued the Dhc mislocalization phenotype observed in $Gl^{G38S}/Gl^{\Delta 22}$ animals (Figure 7F). These data show that TB Dhc accumulation is specific to the motor-neuron disease-associated mutation in p150, and therefore these results identify a key distinction between different mutations, both within the p150 CAP-Gly domain, that cause two distinct human neurodegenerative diseases.

blot analysis shows that $p150^{G38S}$-HA is expressed at lower levels than $p150^{G50A}$ and $p150^{G50R}$, which are expressed at lower levels than $p150^{WT}$. A $p150^{G38S}$-*HA* transgenic line with a duplication of the P element insertion and a robust level of p150 expression ($G38S^{Hi}$) was used to control for protein levels.

(D) HA-tagged $p150^{WT}$ and $p150^{G50R}$ are diffusely expressed in the cytoplasm of motor neurons when expressed with *OK371-GAL4*, whereas $p150^{G38S}$ forms cytoplasmic aggregates.

(E and F) Overexpression of Perry mutant forms of p150 (G50A and G50R) does not cause the dynein TB phenotype observed with overexpression of $p150^{G38S}$. Furthermore, Perry mutant forms of p150 can rescue the dynein mislocalization phenotype seen in $Gl^{G38S}/Gl^{\Delta 22}$ animals. Quantitation performed as in Figures 5C and 5D. Scale bar represents 5 μm. *$p < 0.01$; **$p < 0.0001$. Error bars represent SEM.

DISCUSSION

To better understand the underlying cause of neurodegenerative diseases resulting from mutations in the CAP-Gly domain of the dynactin subunit p150, we introduced disease-associated p150^{Glued} mutations into *Drosophila* by using homologous recombination and transgenesis. Interestingly, p150 is enriched at MT plus ends of NMJ TBs, and *Gl*^{G38S} larvae develop TB swellings and accumulation of the retrograde motor dynein. We find strong synergistic genetic interactions between *khc* and *glued* that produce phenotypes at TBs, suggesting that p150-mediated coordination of bidirectional axonal transport occurs at synaptic termini. Our data suggest that the CAP-Gly domain of p150 is required for initiation of dynein-mediated retrograde transport at terminal boutons.

p150 Regulates Dynein-Mediated Retrograde Transport at Synaptic Termini

We demonstrate here that p150 is enriched at TB microtubule plus ends, consistent with the known function of CAP-Gly domain-containing proteins. Localization of p150 at plus ends has been observed in nonneuronal cells (Habermann et al., 2001; Vaughan et al., 1999, 2002; Zhang et al., 2003), and dynein localization to plus ends in *Aspergillus* requires p150 (Xiang et al., 2000). The p150 microtubule-binding domain has been proposed to regulate the processivity of retrograde microtubule transport via a ''skating'' mechanism (Culver-Hanlon et al., 2006). However, analysis of microtubule transport in S2 cells lacking the MT-binding domain demonstrates normal minus-end-directed transport (Kim et al., 2007). Furthermore, in budding yeast, the *G59S* mutation or CAP-Gly deletion mutants disrupt nuclear migration, but not other dynein-dependent transport events (Moore et al., 2009). Our analysis of endosomal axon transport in *Gl*^{G38S} animals further suggests that loss of p150 microtubule binding ability does not affect minus-end-directed transport in axons.

The accumulation of dynein and kinesin motor proteins, as well as endosomal vesicles, specifically within the TB of *Glued* mutants suggests that dynactin may function to coordinate retrograde transport at TBs. Indeed, by using live imaging at the NMJ, we show that disruption of dynactin causes accumulation of dense core vesicles at TBs, and these DCVs fail to undergo retrograde transport out of this distal-most synaptic bouton. These data directly demonstrate that dynactin plays a critical role in regulating retrograde transport at TBs.

Why are retrograde transport defects seen specifically at *Gl*^{G38S} TBs and not along axons, which also have MT plus ends? There are at least two (nonmutually exclusive) explanations for this observation. (1) TBs have dynamic MTs but lack stabilized MT bundles (Pawson et al., 2008). In this model, microtubule-associated protein (MAP)-stabilized MTs may recruit motors and cargo independent of dynactin and compensate for the disruption of MT binding by p150 along the axon and in proximal boutons; indeed, MAPs can directly associate with dynein and kinesin (Jiménez-Mateos et al., 2005; Sung et al., 2008). (2) Retrograde transport initiation rates are much higher at TBs than in proximal boutons or axons (Wong et al., 2012). In this model, continuous anterograde transport of vesicles to TBs may overwhelm the ability of cargo to undergo p150-independent capture for subsequent retrograde transport at *Gl*^{G38S} TBs. Because retrograde endosomal transport may occur normally in *Gl*^{G38S} mutants from proximal boutons (which comprise the overwhelming majority of boutons at the NMJ), this may explain why we do not observe a disruption of retrograde transport along axons.

What is the mechanism whereby p150 regulates retrograde transport at terminal boutons? Growing microtubules are dynamically unstable, and minus-end-directed microtubule transport of Golgi membranes is initiated upon contact with microtubule plus ends, a process that requires p150 (Vaughan et al., 2002). We propose that a similar ''search and capture'' mechanism occurs at synaptic termini, whereby growing microtubules explore the terminal bouton and, upon contact with the dynactin/dynein complex, cargo are recruited for retrograde transport (Figure 8). A similar model has been proposed for dynactin +TIP function in nonneuronal cells (Vaughan, 2004; Wu et al., 2006). Though dynamic MT plus ends are observed throughout axons and the NMJ (Pawson et al., 2008), we propose that they are uniquely required for retrograde transport at synaptic termini, which lack stable microtubule bundles.

Kinesin and p150^{Glued} Function Cooperatively at Synaptic Termini

Our genetic analyses demonstrate a strong synergistic interaction between kinesin and dynactin at NMJ synapses, the opposite of what one would predict if these proteins solely functioned in unidirectional anterograde or retrograde axonal transport, respectively. The dynein/dynactin complex requires kinesin for anterograde transport along axons, and the interaction between dynein at plus ends and early endosomes in *Aspergillus* requires kinesin (Zhang et al., 2010). Thus, kinesin may be required to localize the dynactin/dynein complex to microtubule plus ends at synapses, where it captures vesicular cargo for the initiation of retrograde transport (Figure 8). Therefore, kinesin-mediated delivery of dynein/dynactin to plus ends likely allows for coordination of kinesin-mediated anterograde transport and dynein-mediated retrograde transport at synapses.

How Does Disruption of p150 Affect Synapse Function?

We show here that loss of dynactin in *Drosophila* motor neurons causes a robust accumulation of endosomal membranes specifically within swollen NMJ TBs. Interestingly, these phenotypes are most severe in distal abdominal larval segments, similar to the distal-predominant symptoms observed in patients. Our live imaging of DCV transport at TBs suggests that these phenotypes are due to a defect in retrograde transport from the TB. In *Gl*^{G38S} animals, we see a reduction in evoked neurotransmitter release, despite normal spontaneous release. This physiologic phenotype is reminiscent of Rab5 mutants, which are defective in endosomal trafficking at synapses (Wucherpfennig et al., 2003). Overexpression of p150$^{\Delta C}$ causes a reduction in evoked neurotransmitter release due to presynaptic retractions (Eaton et al., 2002). In contrast, our *Gl*^{G38S} mutants do not exhibt a decrease in the number of synaptic boutons at the larval NMJ; rather, *Gl*^{G38S} mutants develop TB swelling and accumulation of endosomal membranes. NMJ TBs exhibit greater neurotransmitter exocytosis than proximal boutons (Guerrero et al.,

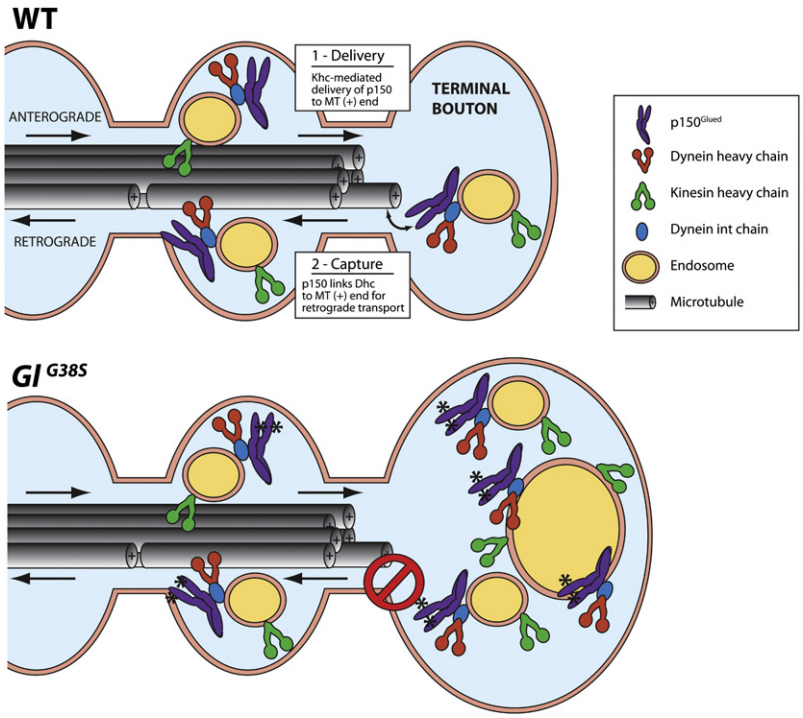

Figure 8. Model for p150^{Glued} Function at Synaptic Termini

Kinesin (Khc) is required for delivery of p150^{Glued} and dynein (Dhc) to microtubule plus ends at NMJ terminal boutons (TBs) (1). Dynamically elongating microtubules may explore the TB and become stabilized through interactions between MT plus ends and the CAP-Gly domain of p150^{Glued}. This interaction allows dynein to initiate minus-end-directed retrograde endosomal transport, possibly by capturing small endosomal vesicles that have recently undergone endocytosis (2). This function of p150 is specifically disrupted by mutations in the CAP-Gly domain that cause motor neuron disease (G59S). In *Gl^{G38S}* larvae, the microtubule-binding function of the CAP-Gly domain of p150 is disrupted at synaptic termini, leading to an accumulation of enlarged endosomal vesicles and the kinesin and dynein motors. Error bars represent SEM.

2005), and TBs are critical for DCV circulation to proximal boutons (Wong et al., 2012). Because endosomes are hypothesized to be important sorting stations for synaptic vesicle proteins (Bonanomi et al., 2006; Hoopmann et al., 2010; Uytterhoeven et al., 2011), we suggest that the impairment in neurotransmitter release is due to a disruption of synaptic vesicle sorting or release at TBs.

Mechanism Underlying Motor Neuron Degeneration in HMN7B

A central hypothesis that explains how mutations in the dynein/dynactin complex cause motor neuron degenerative disease postulates that disruption of dynein-mediated retrograde axonal transport underlies these diseases (Perlson et al., 2010). However, no biochemical evidence of axonal transport disruption was observed in transgenic mice expressing p150^{G59S} (Chevalier-Larsen et al., 2008). Similarly, we show here that axonal transport of endosomes, and also retrograde endosomal signaling, is not disrupted in *Gl^{G38S}* animals. Thus, mutations in the CAP-Gly domain of p150 do not apparently affect cargo transport along MTs; our data suggest that the HMN7B mutation specifically disrupts p150 function at MT plus ends of synapses.

How does disruption of MT plus-end binding lead to neurodegeneration? Presynaptic retractions that occur early in the pathogenesis of motor neuron degenerative disease (Fischer et al., 2004) start at the distal-most end of synapses and are observed in larvae with severe disruption of p150^{Glued} (Eaton et al., 2002). Therefore, one potential mechanism is that the terminal bouton phenotypes we observe here lead to synapse instability and retraction with aging. Alternatively, the dynactin/dynein complex is believed to mediate minus-end-directed microtubule-based transport of multiple cargos throughout neurons, including ER, Golgi, and mitochondria. We cannot exclude the possibility that a function of p150^{Glued} not assayed in this study is also disrupted by these mutations and is more relevant to the pathogenesis of disease.

Both HMN7B and Perry syndrome are caused by dominant mutations in p150, and the mechanisms by which these mutations cause disease are unknown. Most dominantly inherited neurodegenerative diseases (for example, ALS caused by SOD mutations and polyglutamine expansion diseases) are caused by gain of a toxic function. Our analysis of the HMN7B mutation in flies does not provide evidence for a gain of function. Instead, we demonstrate that the disease-causing mutations in p150 result in a partial loss of *Glued* function, and they may also function in a dominant-negative fashion when overexpressed. This is consistent with the severe phenotypes seen in transgenic mice when p150^{G59S} is overexpressed (Chevalier-Larsen et al., 2008; Laird et al., 2008). Thus, our data suggest that a loss-of-function and/or dominant-negative mechanism causes HMN7B motor neuron disease.

Although further analysis of adult *Gl^{G38S}* flies will be required to determine how well they model HMN7B pathologically, several of our findings indicate that this model does share features with human motor neuron diseases, including aggregation of mutant protein within motor neurons, adult-onset locomotor impairment, and a deficit in synaptic transmission at the NMJ. How mutations in ubiquitously expressed proteins cause degeneration of specific neuronal subtypes is a fundamental question that must be addressed if we are to understand the etiology of neurodegenerative diseases. In inherited neuropathies, the long axonal length of motor neurons that innervate distal limb muscles is believed to underlie the length-dependent pathology (Hirokawa et al., 2010); however, in most neurodegenerative diseases, including HMN7B and Perry syndrome, the reason that specific neurons are affected is unknown. The identification of mutations within the same domain of the same protein that cause two distinct neurodegenerative syndromes provides a unique opportunity to understand how these mutations

differentially affect protein function, and our data lend insight into the molecular mechanisms underlying the cell-type specificity of distinct neurodegeneration syndromes.

The G59S mutation is predicted to destabilize the CAP-Gly domain, whereas the Perry mutations all lie on the surface of this domain. Destabilization of the CAP-Gly domain by the G59S mutation may make it more susceptible to aggregation, as we observe here in *Drosophila* motor neurons. Furthermore, it is likely that distinct protein-protein interactions are disrupted by these different mutations. We only observe an accumulation of dynein at synaptic termini after overexpression of the HMN7B mutant forms of p150 and not the Perry mutations. We propose that specific disruption of the interaction between p150 and microtubule ends at synaptic termini underlies the motor neuron specificity of neurodegeneration in HMN7B.

EXPERIMENTAL PROCEDURES

Fly Strains

All crosses were performed at 25°C. *Canton-S* and w^{1118} were used as wild-type control lines. The human $p150^{WT}$ and $p150^{G59S}$ constructs were generated by cloning C-terminal flag-tagged p150 cDNA obtained from P. Wong (Laird et al., 2008) into pUAST. The G38S mutation was generated in the *Drosophila p150* cDNA (RE24170) by using the Stratagene Quick-change mutagenesis kit. The Gl^{G38S} knockin allele was generated as described (Rong et al., 2002 and Supplemental Experimental Procedures). The Gl^{1} and Gl^{1-3} alleles were provided by T. Hays (Martin et al., 1999); $Gl^{\Delta 22}$ (Siller et al., 2005) and *UAS-GFP:Gl* (full length [aa1-1265] and ΔMB [aa201-1265]) were generously provided by C. Doe. Additional lines are described in Supplemental Experimental Procedures.

Biochemistry, Immunohistochemistry, and Imaging

Microtubule-associated proteins from adult flies collected 16 hr after a 1 hr, 37°C heat shock to induce GAL4 expression were purified from fly extracts as described (McGrail et al., 1995). NMJ analysis was limited to muscle 4 unless stated otherwise. Antibodies used are detailed in Supplemental Experimental Procedures. A synapse was considered to have TB anti-HRP or anti-Dhc accumulation if the fluorescence intensity within the TB was clearly much higher than in proximal boutons. Fluorescent images were acquired by using a Zeiss LSM 510 confocal microscope using a PLAN-APO 63×, 1.4 NA oil-immersion objective. Maximum-intensity Z projections of confocal stacks were generated and processed by using Adobe Photoshop. Intensity measurements and NMJ TB volume were obtained by thresholding with Imaris software. For scanning electron microscopy, fly heads were coated with gold:palladium by using a vacuum evaporator and imaged immediately by using a LEO/Zeiss Field-Emission SEM.

SPAIM experiments were performed as described (Wong et al., 2012). For other live-imaging experiments, we rinsed wandering third-instar larvae and pinned them in Ca^{2+}-free HL3 on the sylgard insert of a custom-made imaging mount, placed a coverslip over the preparation, and secured it. Imaging of axonal transport was performed on a Zeiss Axio Observer with a 40× oil objective (EC Plan-Neofluar 1.3 NA) and collected on an AxioCAM charge-coupled device camera. Movies were analyzed as described (Louie et al., 2008). For ANF:GFP fluorescence recovery after photobleaching (FRAP) experiments, we acquired spinning-disc confocal images of dense-core vesicles at muscle 6/7 NMJs by using a Zeiss Axio Imager Z1 microscope and 63× 1.4 NA oil-immersion objective and collected them on a QuantEM 512SC camera (Photometrics). ANF:GFP in proximal boutons was bleached by using a 488 nm laser controlled by a Mosaic Digital Illumination System (Photonic Instruments).

Electrophysiology and Statistics

Electrophysiological recordings from muscle 6, segment A3, were performed as described (Imlach and McCabe, 2009). Data are expressed as mean ± SEM. A Student's t test was performed for pairwise comparisons between each genotype and its wild-type control by using GraphPad Prism.

SUPPLEMENTAL INFORMATION

Supplemental Information includes eight figures, Supplemental Experimental Procedures, and five movies and can be found with this article online at doi:10.1016/j.neuron.2012.02.026.

ACKNOWLEDGMENTS

We are grateful to Chris Doe, Vladimir Gelfand, Tom Hays, Rod Murphey, Phil Wong, Sangyun Jeong, and Herman Aberle for reagents. We thank Ben Choi for pMad work and Manish Jaiswal and Vafa Bayat for helpful comments. We thank Erik Griffin, Geraldine Seydoux, Norm Haughey, Terry Shelley, Michele Pucak, and the NINDS Multi-photon Core Facility (MH084020) at JHMI for assistance with imaging. We also thank the BDSC, VDRC, and DGRC for fly stocks and reagents. This work was funded by the Packard Center for ALS Research (A.L.K. and T.E.L.), P2ALS (B.D.M.), NINDS K08-NS062890 to T.E.L., R01-NS35165 to A.L.K, and RO1-NS32385 to M.Y.W. and E.S.L. A.L.K. is an Investigator of the Howard Hughes Medical Institute.

Accepted: February 28, 2012
Published: April 25, 2012

REFERENCES

Allen, M.J., Shan, X., Caruccio, P., Froggett, S.J., Moffat, K.G., and Murphey, R.K. (1999). Targeted expression of truncated glued disrupts giant fiber synapse formation in Drosophila. J. Neurosci. *19*, 9374–9384.

Bischof, J., Maeda, R.K., Hediger, M., Karch, F., and Basler, K. (2007). An optimized transgenesis system for Drosophila using germ-line-specific phiC31 integrases. Proc. Natl. Acad. Sci. USA *104*, 3312–3317.

Bonanomi, D., Benfenati, F., and Valtorta, F. (2006). Protein sorting in the synaptic vesicle life cycle. Prog. Neurobiol. *80*, 177–217.

Burkhardt, J.K., Echeverri, C.J., Nilsson, T., and Vallee, R.B. (1997). Overexpression of the dynamitin (p50) subunit of the dynactin complex disrupts dynein-dependent maintenance of membrane organelle distribution. J. Cell Biol. *139*, 469–484.

Chevalier-Larsen, E.S., Wallace, K.E., Pennise, C.R., and Holzbaur, E.L. (2008). Lysosomal proliferation and distal degeneration in motor neurons expressing the G59S mutation in the p150Glued subunit of dynactin. Hum. Mol. Genet. *17*, 1946–1955.

Clark, I., Giniger, E., Ruohola-Baker, H., Jan, L.Y., and Jan, Y.N. (1994). Transient posterior localization of a kinesin fusion protein reflects anteroposterior polarity of the Drosophila oocyte. Curr. Biol. *4*, 289–300.

Culver-Hanlon, T.L., Lex, S.A., Stephens, A.D., Quintyne, N.J., and King, S.J. (2006). A microtubule-binding domain in dynactin increases dynein processivity by skating along microtubules. Nat. Cell Biol. *8*, 264–270.

De Vos, K.J., Grierson, A.J., Ackerley, S., and Miller, C.C. (2008). Role of axonal transport in neurodegenerative diseases. Annu. Rev. Neurosci. *31*, 151–173.

Deacon, S.W., Serpinskaya, A.S., Vaughan, P.S., Lopez Fanarraga, M., Vernos, I., Vaughan, K.T., and Gelfand, V.I. (2003). Dynactin is required for bidirectional organelle transport. J. Cell Biol. *160*, 297–301.

Deinhardt, K., Salinas, S., Verastegui, C., Watson, R., Worth, D., Hanrahan, S., Bucci, C., and Schiavo, G. (2006). Rab5 and Rab7 control endocytic sorting along the axonal retrograde transport pathway. Neuron *52*, 293–305.

Desai, C.J., Popova, E., and Zinn, K. (1994). A Drosophila receptor tyrosine phosphatase expressed in the embryonic CNS and larval optic lobes is a member of the set of proteins bearing the "HRP" carbohydrate epitope. J. Neurosci. *14*, 7272–7283.

Eaton, B.A., Fetter, R.D., and Davis, G.W. (2002). Dynactin is necessary for synapse stabilization. Neuron *34*, 729–741.

Farrer, M.J., Hulihan, M.M., Kachergus, J.M., Dächsel, J.C., Stoessl, A.J., Grantier, L.L., Calne, S., Calne, D.B., Lechevalier, B., Chapon, F., et al. (2009). DCTN1 mutations in Perry syndrome. Nat. Genet. *41*, 163–165.

Fischer, L.R., Culver, D.G., Tennant, P., Davis, A.A., Wang, M., Castellano-Sanchez, A., Khan, J., Polak, M.A., and Glass, J.D. (2004). Amyotrophic lateral sclerosis is a distal axonopathy: evidence in mice and man. Exp. Neurol. *185*, 232–240.

Gross, S.P., Welte, M.A., Block, S.M., and Wieschaus, E.F. (2002). Coordination of opposite-polarity microtubule motors. J. Cell Biol. *156*, 715–724.

Guerrero, G., Reiff, D.F., Agarwal, G., Ball, R.W., Borst, A., Goodman, C.S., and Isacoff, E.Y. (2005). Heterogeneity in synaptic transmission along a Drosophila larval motor axon. Nat. Neurosci. *8*, 1188–1196.

Haass, C., Koo, E.H., Mellon, A., Hung, A.Y., and Selkoe, D.J. (1992). Targeting of cell-surface beta-amyloid precursor protein to lysosomes: alternative processing into amyloid-bearing fragments. Nature *357*, 500–503.

Habermann, A., Schroer, T.A., Griffiths, G., and Burkhardt, J.K. (2001). Immunolocalization of cytoplasmic dynein and dynactin subunits in cultured macrophages: enrichment on early endocytic organelles. J. Cell Sci. *114*, 229–240.

Haghnia, M., Cavalli, V., Shah, S.B., Schimmelpfeng, K., Brusch, R., Yang, G., Herrera, C., Pilling, A., and Goldstein, L.S. (2007). Dynactin is required for coordinated bidirectional motility, but not for dynein membrane attachment. Mol. Biol. Cell *18*, 2081–2089.

Hirokawa, N., Niwa, S., and Tanaka, Y. (2010). Molecular motors in neurons: transport mechanisms and roles in brain function, development, and disease. Neuron *68*, 610–638.

Honnappa, S., Okhrimenko, O., Jaussi, R., Jawhari, H., Jelesarov, I., Winkler, F.K., and Steinmetz, M.O. (2006). Key interaction modes of dynamic +TIP networks. Mol. Cell *23*, 663–671.

Hoopmann, P., Punge, A., Barysch, S.V., Westphal, V., Bückers, J., Opazo, F., Bethani, I., Lauterbach, M.A., Hell, S.W., and Rizzoli, S.O. (2010). Endosomal sorting of readily releasable synaptic vesicles. Proc. Natl. Acad. Sci. USA *107*, 19055–19060.

Imlach, W., and McCabe, B.D. (2009). Electrophysiological methods for recording synaptic potentials from the NMJ of Drosophila larvae. J. Vis. Exp. *24*, e1109.

Jiménez-Mateos, E.M., Wandosell, F., Reiner, O., Avila, J., and González-Billault, C. (2005). Binding of microtubule-associated protein 1B to LIS1 affects the interaction between dynein and LIS1. Biochem. J. *389*, 333–341.

Kardon, J.R., and Vale, R.D. (2009). Regulators of the cytoplasmic dynein motor. Nat. Rev. Mol. Cell Biol. *10*, 854–865.

Kim, H., Ling, S.C., Rogers, G.C., Kural, C., Selvin, P.R., Rogers, S.L., and Gelfand, V.I. (2007). Microtubule binding by dynactin is required for microtubule organization but not cargo transport. J. Cell Biol. *176*, 641–651.

Lai, C., Lin, X., Chandran, J., Shim, H., Yang, W.J., and Cai, H. (2007). The G59S mutation in p150(glued) causes dysfunction of dynactin in mice. J. Neurosci. *27*, 13982–13990.

Laird, F.M., Farah, M.H., Ackerley, S., Hoke, A., Maragakis, N., Rothstein, J.D., Griffin, J., Price, D.L., Martin, L.J., and Wong, P.C. (2008). Motor neuron disease occurring in a mutant dynactin mouse model is characterized by defects in vesicular trafficking. J. Neurosci. *28*, 1997–2005.

Levitan, E.S., Lanni, F., and Shakiryanova, D. (2007). In vivo imaging of vesicle motion and release at the Drosophila neuromuscular junction. Nat. Protoc. *2*, 1117–1125.

Levy, J.R., Sumner, C.J., Caviston, J.P., Tokito, M.K., Ranganathan, S., Ligon, L.A., Wallace, K.E., LaMonte, B.H., Harmison, G.G., Puls, I., et al. (2006). A motor neuron disease-associated mutation in p150Glued perturbs dynactin function and induces protein aggregation. J. Cell Biol. *172*, 733–745.

Louie, K., Russo, G.J., Salkoff, D.B., Wellington, A., and Zinsmaier, K.E. (2008). Effects of imaging conditions on mitochondrial transport and length in larval motor axons of Drosophila. Comp. Biochem. Physiol. A Mol. Integr. Physiol. *151*, 159–172.

Martin, M., Iyadurai, S.J., Gassman, A., Gindhart, J.G., Jr., Hays, T.S., and Saxton, W.M. (1999). Cytoplasmic dynein, the dynactin complex, and kinesin are interdependent and essential for fast axonal transport. Mol. Biol. Cell *10*, 3717–3728.

McCabe, B.D., Marqués, G., Haghighi, A.P., Fetter, R.D., Crotty, M.L., Haerry, T.E., Goodman, C.S., and O'Connor, M.B. (2003). The BMP homolog Gbb provides a retrograde signal that regulates synaptic growth at the Drosophila neuromuscular junction. Neuron *39*, 241–254.

McGrail, M., Gepner, J., Silvanovich, A., Ludmann, S., Serr, M., and Hays, T.S. (1995). Regulation of cytoplasmic dynein function in vivo by the Drosophila Glued complex. J. Cell Biol. *131*, 411–425.

Moore, J.K., Sept, D., and Cooper, J.A. (2009). Neurodegeneration mutations in dynactin impair dynein-dependent nuclear migration. Proc. Natl. Acad. Sci. USA *106*, 5147–5152.

Pawson, C., Eaton, B.A., and Davis, G.W. (2008). Formin-dependent synaptic growth: evidence that Dlar signals via Diaphanous to modulate synaptic actin and dynamic pioneer microtubules. J. Neurosci. *28*, 11111–11123.

Peris, L., Thery, M., Fauré, J., Saoudi, Y., Lafanechère, L., Chilton, J.K., Gordon-Weeks, P., Galjart, N., Bornens, M., Wordeman, L., et al. (2006). Tubulin tyrosination is a major factor affecting the recruitment of CAP-Gly proteins at microtubule plus ends. J. Cell Biol. *174*, 839–849.

Perlson, E., Maday, S., Fu, M.M., Moughamian, A.J., and Holzbaur, E.L. (2010). Retrograde axonal transport: pathways to cell death? Trends Neurosci. *33*, 335–344.

Pilling, A.D., Horiuchi, D., Lively, C.M., and Saxton, W.M. (2006). Kinesin-1 and Dynein are the primary motors for fast transport of mitochondria in Drosophila motor axons. Mol. Biol. Cell *17*, 2057–2068.

Puls, I., Jonnakuty, C., LaMonte, B.H., Holzbaur, E.L., Tokito, M., Mann, E., Floeter, M.K., Bidus, K., Drayna, D., Oh, S.J., et al. (2003). Mutant dynactin in motor neuron disease. Nat. Genet. *33*, 455–456.

Rolls, M.M., Satoh, D., Clyne, P.J., Henner, A.L., Uemura, T., and Doe, C.Q. (2007). Polarity and intracellular compartmentalization of Drosophila neurons. Neural Dev. *2*, 7.

Rong, Y.S., Titen, S.W., Xie, H.B., Golic, M.M., Bastiani, M., Bandyopadhyay, P., Olivera, B.M., Brodsky, M., Rubin, G.M., and Golic, K.G. (2002). Targeted mutagenesis by homologous recombination in D. melanogaster. Genes Dev. *16*, 1568–1581.

Roos, J., Hummel, T., Ng, N., Klämbt, C., and Davis, G.W. (2000). Drosophila Futsch regulates synaptic microtubule organization and is necessary for synaptic growth. Neuron *26*, 371–382.

Siller, K.H., Serr, M., Steward, R., Hays, T.S., and Doe, C.Q. (2005). Live imaging of Drosophila brain neuroblasts reveals a role for Lis1/dynactin in spindle assembly and mitotic checkpoint control. Mol. Biol. Cell *16*, 5127–5140.

Sung, H.H., Telley, I.A., Papadaki, P., Ephrussi, A., Surrey, T., and Rørth, P. (2008). Drosophila ensconsin promotes productive recruitment of Kinesin-1 to microtubules. Dev. Cell *15*, 866–876.

Swaroop, A., Paco-Larson, M.L., and Garen, A. (1985). Molecular genetics of a transposon-induced dominant mutation in the Drosophila locus Glued. Proc. Natl. Acad. Sci. USA *82*, 1751–1755.

Takei, K., Mundigl, O., Daniell, L., and De Camilli, P. (1996). The synaptic vesicle cycle: a single vesicle budding step involving clathrin and dynamin. J. Cell Biol. *133*, 1237–1250.

Uytterhoeven, V., Kuenen, S., Kasprowicz, J., Miskiewicz, K., and Verstreken, P. (2011). Loss of skywalker reveals synaptic endosomes as sorting stations for synaptic vesicle proteins. Cell *145*, 117–132.

Vaughan, K.T. (2004). Surfing, regulating and capturing: are all microtubule-tip-tracking proteins created equal? Trends Cell Biol. *14*, 491–496.

Vaughan, K.T., Tynan, S.H., Faulkner, N.E., Echeverri, C.J., and Vallee, R.B. (1999). Colocalization of cytoplasmic dynein with dynactin and CLIP-170 at microtubule distal ends. J. Cell Sci. *112*, 1437–1447.

Vaughan, P.S., Miura, P., Henderson, M., Byrne, B., and Vaughan, K.T. (2002). A role for regulated binding of p150(Glued) to microtubule plus ends in organelle transport. J. Cell Biol. *158*, 305–319.

Waterman-Storer, C.M., and Holzbaur, E.L. (1996). The product of the Drosophila gene, Glued, is the functional homologue of the p150Glued component of the vertebrate dynactin complex. J. Biol. Chem. *271*, 1153–1159.

Weisbrich, A., Honnappa, S., Jaussi, R., Okhrimenko, O., Frey, D., Jelesarov, I., Akhmanova, A., and Steinmetz, M.O. (2007). Structure-function relationship of CAP-Gly domains. Nat. Struct. Mol. Biol. *14*, 959–967.

Wong, M.Y., Zhou, C., Shakiryanova, D., Lloyd, T.E., Deitcher, D.L., and Levitan, E.S. (2012). Neuropeptide delivery to synapses by long-range vesicle circulation and sporadic capture. Cell *148*, 1029–1038.

Wu, X., Xiang, X., and Hammer, J.A., 3rd. (2006). Motor proteins at the microtubule plus-end. Trends Cell Biol. *16*, 135–143.

Wucherpfennig, T., Wilsch-Bräuninger, M., and González-Gaitán, M. (2003). Role of Drosophila Rab5 during endosomal trafficking at the synapse and evoked neurotransmitter release. J. Cell Biol. *161*, 609–624.

Xiang, X., Han, G., Winkelmann, D.A., Zuo, W., and Morris, N.R. (2000). Dynamics of cytoplasmic dynein in living cells and the effect of a mutation in the dynactin complex actin-related protein Arp1. Curr. Biol. *10*, 603–606.

Zhang, J., Li, S., Fischer, R., and Xiang, X. (2003). Accumulation of cytoplasmic dynein and dynactin at microtubule plus ends in Aspergillus nidulans is kinesin dependent. Mol. Biol. Cell *14*, 1479–1488.

Zhang, J., Zhuang, L., Lee, Y., Abenza, J.F., Peñalva, M.A., and Xiang, X. (2010). The microtubule plus-end localization of Aspergillus dynein is important for dynein-early-endosome interaction but not for dynein ATPase activation. J. Cell Sci. *123*, 3596–3604.